COMPUTER-AIDED DESIGN & APPLICATIONS, 2017
VOL. 14, NO. 6, 833–843
https://doi.org/10.1080/16864360.2017.1287759

Novel surgical needle design and manufacturing for vibratory-assisted insertion in medical applications

Yi Cai [a], Jason Moore [b] and Yuan-Shin Lee [a]

[a]North Carolina State University, USA; [b]Pennsylvania State University, USA

ABSTRACT

This paper presents a novel design of solid surgical needle featured by its 4-bevel tip and shaft slots with the aim to further explore the potential of vibratory needle insertion for medical applications. The design philosophy was discussed, and a new way of using electric discharging machining (EDM) is introduced for fabricating the new needle design. Two sets of needle prototypes with different geometry parameters were fabricated and used for insertion into porcine skin with ultrasonic vibration. Modal analysis was conducted for the needles under the given vibration condition. The results showed that the needle design could reduce the puncture force by 14.5% at maximum than the 12.2% of control. The reduction of puncture force was found to be related to the axial displacement or the combination of axial and transverse displacement. The effects of geometry parameters on transverse displacement were also discussed. The presented new design and manufacturing techniques can be used for surgical tools development and medical applications.

KEYWORDS

Design and manufacturing; vibratory needle insertion; analytical modeling; biomedical applications

1. Introduction

Needles are among the most widely used medical devices, and they serve in a wide variety of medical procedures, from ordinary ones like blood sampling and drug delivery to advanced ones like tissue biopsy and brachytherapy [1]. Depending on the specific procedure, a medical needle may come in a solid or a hollow configuration, and sometimes hollow and solid needles are used together as cannula and stylet. Whatever the configuration is, low insertion force is desirable because it helps to reduce tissue deflection and needle bending, so that the placement accuracy of the needle can be improved and the insertion injury has the potential to recover better [5]. Low insertion force also reduces the pain sensed by patients, which is very important when anesthesia is not applicable [6]. A good example to illustrate the importance of low insertion force is in brachytherapy, where radioactive seeds are placed systematically in a diseased organ to kill cancer cells. Accurate seed placement is critical to ensure the seeds are within the cancer areas requiring treatment and far away enough from healthy cells. However, insertion force not only causes the needle to deflect and bend, but also pushes the target area away from its original location, which will result in incorrect placement and even medical complication. Low insertion force is desirable to minimize such deflection and displacement.

The deflection and insertion force of needle into tissue has been extensively explored in a number of studies for solid needles. Podder *et al.* [22] and Maurin *et al.* [14] investigated the solid needle force with in vivo experiments. O'Leary *et al.* [19] and Podder *et al.* [21] studied the effects of tip geometry on solid needle deflection and force experimentally, while Okamura *et al.* [20] and Webster *et al.* [27] worked on modeling such force and deflection. For hollow needles, Moore *et al.* [18] derived the mathematical models of the inclination angle and the rake angle for plane needle cutting edges, and developed a novel enhanced cutting edge for two-plane symmetric needle [17], which could reduce the insertion force while increasing biopsy sample length. They also utilized a mechanistic approach based on the concept of elementary cutting tool to predict the initial peak needle insertion force [16], and proposed a method to find out the optimal design of two lancet needles with minimal insertion force and bevel length respectively [26]. Fracture mechanics based models have also been developed by incorporating the tissues fracture toughness, shear modulus, and friction force into understanding the total needle insertion force [2]. Since lower insertion force is often associated with smaller needle diameter, micro needles, which are sometimes only 100 μm in diameter, have been able to be fabricated in recent years [4]. While their

CONTACT Yi Cai ycai6@ncsu.edu; Jason Moore jzm14@psu.edu; Yuan-Shin Lee yslee@ncsu.edu

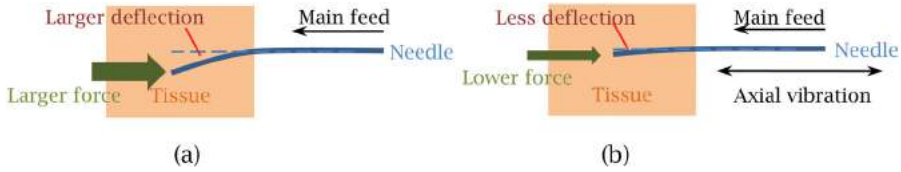

Figure 1. Medical needle insertion: (a) traditional insertion and (b) vibration-assisted insertion.

effects on insertion force reduction are drastic, they are not preferred in situations where a large dose is required or large particulates need to pass through the needle [10].

Vibration-assisted cutting has been used in advanced manufacturing processes, where a high frequency vibration with small amplitude is added to the main feed motion of the cutting tool, as shown in Fig. 1. In drilling, for example, studies have shown that ultrasonic vibrations in the feed direction could reduce burrs in drilling [25], create a better surface finish [12], and reduce the cutting force needed [23]. In our earlier research [11], vibration assisted drilling was studied and an analytical modeling was developed for vibration assisted drilling on bones and metals. In tissue cutting, increased insertion speed has been shown to reduce both insertion force [7] and tissue deflection [13], but higher insertion speed often result in more difficulty in control. Vibration, however, offers a method to increase the maximum local insertion speed of the needle tip while maintaining a slow and controllable average insertion rate [25]. Actually, vibration-assisted cutting has been shown to reduce insertion force in tissue cutting by several researchers. Huang et al. [8] studied the frequency response of Gauge 27 bevel needles and showed that ultrasonic vibration could reduce the insertion force. Barnett et al. [3] tested the effectiveness of axial vibration in reducing the insertion force into porcine skin across a range of frequencies, amplitudes and needle sizes, and found that the addition of the vibration was able to reduce the insertion force by up to 35%. For micro needles, results have shown that the addition of axial vibration can reduce cutting force sometimes up to 70% [28]. From the viewpoint of physics, Khalaji et al. [9] extended the LuGre friction model with high-frequency vibration for translational friction, and demonstrated that it could be reduced with the introduction of low-amplitude vibratory motion onto a regular insertion profile.

This paper presents a novel design of solid surgical needle featured by its 4-bevel tip and shaft slots with the aim to further explore the potential of vibratory needle insertion. The design philosophy of the needle was introduced. To overcome the challenging issues faced in fabricating the designed needles, a non-traditional manufacturing process using electric discharging machining (EDM) for the tip and slots is presented. Needle prototypes of the proposed design were fabricated with different geometries, and they are used to conduct insertion experiment for porcine skin. The puncture force and depth were used to evaluate the performance. The preliminary results showed both weakness and potentials of the proposed design, and indicated the necessity for more experiments. Details of the proposed design and manufacturing processes along with the experimental results are presented in the following sections.

2. Design of the proposed novel surgical needle

To achieve the vibration-assisted surgical needle insertion, a new surgical needle geometry design is proposed to accommodate the vibration during tissue cutting and to amplify the vibration amplitude for more effective cutting. Fig. 2(a) shows the design of the proposed medical needle for vibration-assisted insertion. As shown in Fig. 2(a), the needle tip is featured by the four bevels forming the needle tip and the two slots on the shaft. The bevels are symmetrically distributed in a way that if they are cut by a reference plane perpendicular to the needle central axis, the intersection lines will form a diamond shape, as shown in Fig. 2(b).

In Fig. 2(b), among the four edges formed by the four bevels, the two associated the sharp corners of the diamond shape are the main cutting edges during needle insertion, which are highlighted in the figure. The other two edges only push aside the tissue without cutting. A coordinate system can be built with the Z axis coinciding with central axis of the needle and the X axis passing through the lowest point of the main cutting edges. Actually, the geometry of the needle tip can be determined with only two parameters: the bevel angle φ and the interval angle β. Given CD is perpendicular to AB, φ is defined as the angle between OC and CD, and β is the angle between OD and OB. From an intuitive viewpoint, φ determines the relationship between a bevel and the needle central axis, while β determines the distribution relationship among the four bevels. Just like the

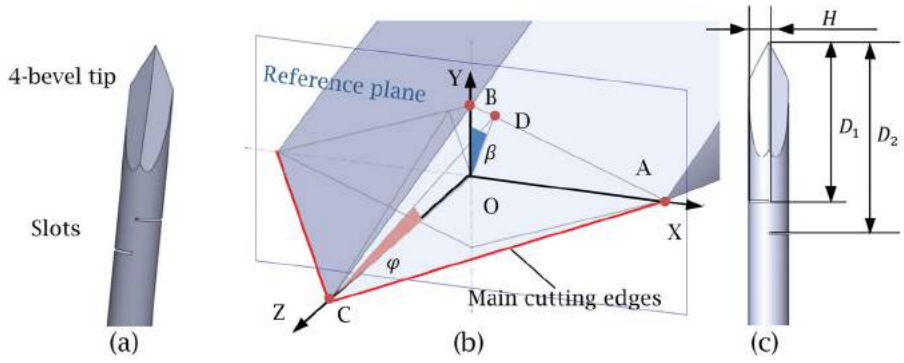

Figure 2. The proposed needle design: (a) overview, (b) tip design, and (c) slot design.

bevel angles in commercial medical needles, the range of φ can be set to be $10^\circ \leq \varphi \leq 30^\circ$. The range of β is $0^\circ < \beta \leq 45^\circ$ within the coordinate system built above. These two parameters are also useful in the fabrication process of the needle, which will be discussed in the next section.

The two slots on the opposite sides of the needle shaft, where lies the major novelty of the proposed design, aim at modifying the stiffness of the needle, and thus the frequency response. The slots are cut along the X axis direction as shown in Fig. 2(c), which enable the main cutting edges to vibrate more easily along the X direction to perform tissue cutting than along the Y direction under stimulation. This explains why a four-bevel design is used instead of the relatively simple tri-bevel needle commonly used in brachytherapy. When the tip of a tri-bevel needle vibrates along a specific direction perpendicular to the central axis, only one cutting edge at maximum can perform tissue cutting, while the bevel between the other two cutting edges will hinder the vibration in that direction. By matching the amplitude and frequency of the vibration applied to the needle in the Z axis direction with the location and depth of the slots, the main cutting edges can vibrate with high speed along the Z and X directions to perform micro tissue cutting, which will be beneficial to reduce the insertion force. An illustrative picture is shown in Fig. 3. The design parameters for the slots include the distance from the needle tip to the first slot, D_1, the distance from the needle tip to the second slot, D_2, and the depth of them, H. Their effects on insertion force will be demonstrated in Section 5.

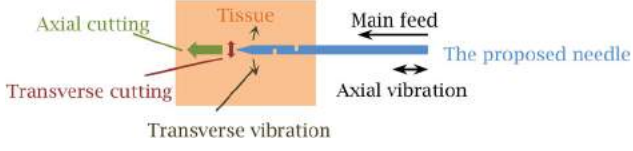

Figure 3. Illustration of insertion with the proposed needle design.

3. Fabrication method of the proposed novel surgical needle

The intricate geometry needle shown in Fig. 1 is challenging to manufacture due to its intricate geometric design and small dimensions. Commercial needle tips are usually generated by a special burr-free grinding process. It can also be applied to process the four bevels of the compliant needle. However, the two small slots on the shaft are difficult to process with traditional grinding. In this paper, after exploring several different processes, it is identified that the forceless electrical discharge machining (EDM) would be an effective and economic solution. As a result, both the bevels and the slots are processed on an EDM machine to avoid the alignment difficulty and inaccuracy caused by transferring the work piece between a grinding and an EDM machine. Details of the machining process are described in the following sections.

3.1. Fabricating the bevels by EDM

The setup of for the EDM of needle bevels is shown in Fig. 4(a). The EDM was conducted in a Charmilles Roboform 3-axis CNC EDM machine. The work piece used was an AISI 304 stainless steel rod with a diameter $D = 1.27$ mm and a length $L = 300$ mm. It was secured to a spin index with a resolution of 1 degree using a 5C collet. The spin index was fixed to a tilting table with bolts and nuts to form a composite structure, and the whole structure was fixed with the bottom of the tilting table clamped to the machine table. The rotation axis of the tilting table was parallel to the Y axis of the EDM machine coordinate system, while the rotation axis of the spin index was perpendicular to that of the tilting table in space. With this setup, the bevel angle φ and the interval angle β can be directly controlled by the rotation of the tilting table and the spin index respectively. The block electrode is made of a copper block milled to a standard rectangle shape.

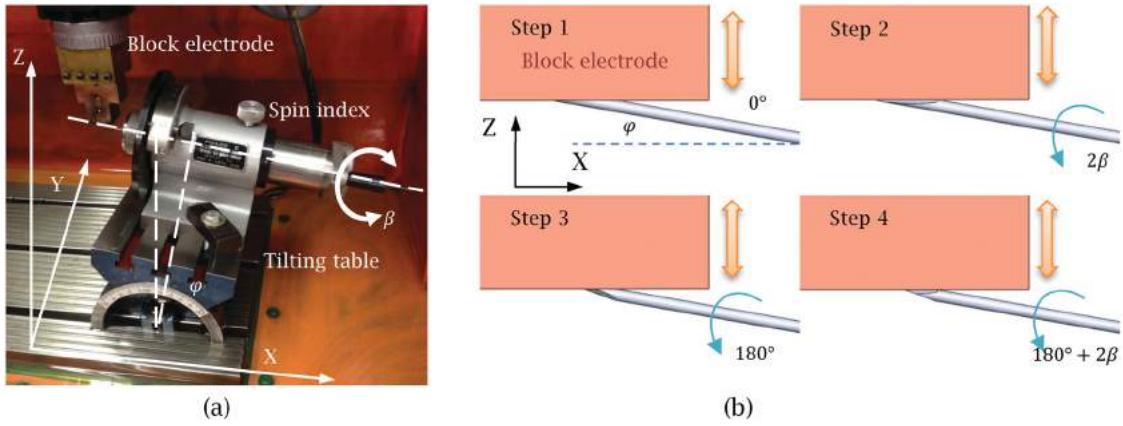

Figure 4. Fabrication of bevels: (a) setup for EDM of needle bevels and (b) the four-step EDM procedure to generate tip bevels.

Fig. 4(b) shows the four-step EDM procedure to generate the bevels on the needle tip. In Step 1, the tilting table was adjusted to bevel angle φ, and the spin index was rotated to the 0° position. The block electrode moved along the negative Z axis of the EDM machine to cut the first bevel needle tip at the end of the work piece. The final Z position of the bottom of the electrode was below the center point at the end of the work piece. In Step 2, the spin indexed was rotated to the 2β position, and the block electrode moved to the same final Z position as in Step 1 to cut the second bevel. In Step 3, the spin indexed was rotated to the 180° position, and the third bevel was cut with the electrode reaching the same final Z position. In Step 4, the spin indexed was rotated to the 180° + 2β position, and the electrode completed the last bevel at the same final Z position. The foil electrode moved along the Y axis of the machine coordinate system after cutting a bevel to make sure each bevel was cut with an unworn section of the block electrode. The needle remains secured to the collet after this step for the following processing of slots.

3.2. Cutting the slots by EDM

Fig. 5(a) shows the setup for the EDM of the slots on the needle shaft. The block electrode was replaced with a foil electrode, which was prepared by using two thin rectangle copper blocks to compress a rectangle pre-flattened copper foil with a thickness of 50 μm. One edge of the foil was extended outside the blocks with a suitable distance (3 mm in this case) to form the cutting edge. Moreover, the tilting table was rotated to the horizontal position so that the rotation axis of the spin index was parallel to the X axis of the machine.

Fig. 5(b) shows the two-step EDM procedure to generate the slots on the needle shaft under the setup above. In Step 1, the spin indexed was rotated to the 90° + β position, and the bottom of the foil electrode moved to a position with a distance of D_1 from the needle tip point to cut the first slot with a depth of H. In Step 2, the spin indexed was rotated to the 270° + β position, and the foil electrode moved along the positive X axis by a distance of D_2 and cut the second slot with a depth of *H*.

Fig. 6(a) shows a prototype of the compliant needle with = 10° $D_1 = 5$ mm, $D_2 = 6$ mm, and H = 0.75D. It can be measured that the width of the slots is about 100 μm, as shown in Fig. 4(b). Such a narrow slot should not trap any tissue during insertion, which would hinder needle movement and cause further damage to the surrounding tissue. The value above is the base line of the achievable slot width with the method described, and wider slots can be fabricated by using multiple foils stacked together if necessary.

4. Insertion experiment for porcine skin

4.1. Experiment setup

Fig. 7 shows the setup for the porcine skin experiment. A porcine skin sample was clamped by two plates using screws on a rotational structure. The plates had 12 aligned holes in them. By rotating the plates together with the skin sample around the central axis, a needle can pass through the skin at 12 different locations without causing any tension to the skin. A linear motor (Dunkermotoren) was utilized to insert the needle into tissue phantom at a constant rate. A six-axis force sensor (ATI) was used to measure the force during insertion, and it was attached to a manual thread guild fixed on an adjacent table for vibration isolation. A data acquisition system (National Instruments, PXIe-6361) and LabVIEW software were used to record the force data and to control the linear motor.

For this study, an ultrasonic piezoelectric transducer (Honda Electronics, Toyohashi, Japan) with a resonance

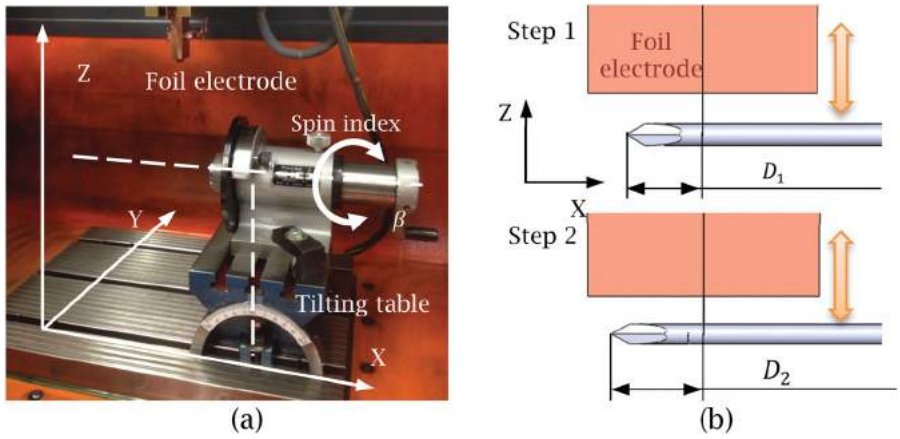

Figure 5. Cutting the slots: (a) setup for EDM of the slots on the needle shaft, and (b) two-step EDM procedure to generate the slots on the needle shaft.

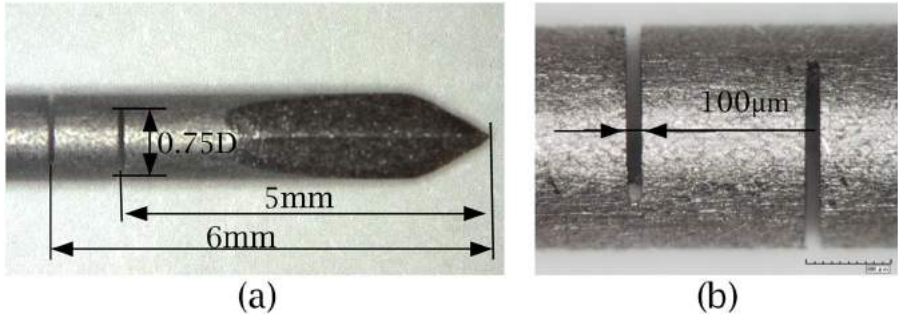

Figure 6. A fabricated example of the proposed design: (a) overview of tip and (b) close view of slots.

frequency of 20 kHz was applied to provide vibration to a needle in the axial direction. Since the actuation amplitude of the piezoelectric ceramics alone was small, a stepped horn made of 6061 aluminum was used to increase the amplitude. A short conical section is added in between the steps to reduce the stress in the horn. A needle could be inserted into the hole at the end of the horn and fixed with screw. An optical probe (MTI Instruments, Albany, NY) was used to measure the peak-to-peak amplitude at the end side of the horn, and the results for different actuation voltages were summarized in Tab. 1. Although a higher actuation voltage resulted

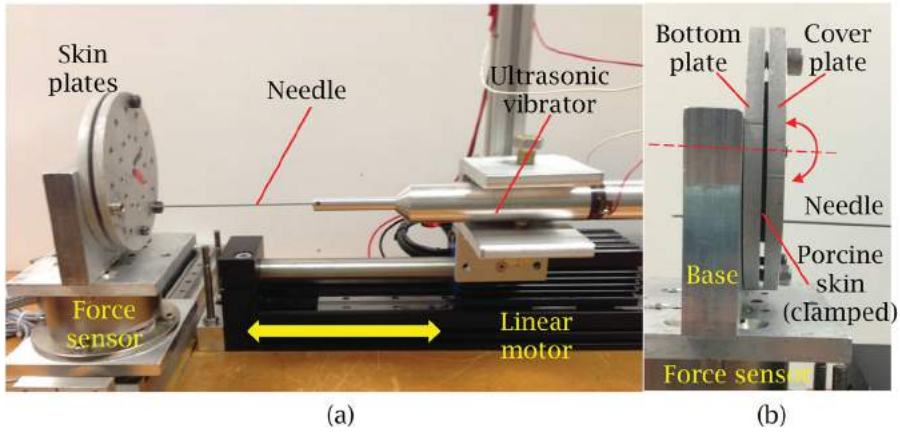

Figure 7. Experiment setup for needle insertion: (a) overview and (b) the skin plates.

in larger amplitude, which may in turn result in lower insertion force, 20 V was used in the experiment for safety considerations.

Table 1. Amplitude of the ultrasonic transducer with horn under different voltages.

Voltage (V)	5	20	25	50	75	100
Amplitude (μm)	5.93	14.83	18.44	32.47	44.93	55.53

4.2. Experiment design

To study the effects of needle geometry parameters on insertion performance, two sets of needle prototypes were fabricated with the methods presented above. They all had a φ of 10°, an β of 20° and a D of 1.27 mm (Gauge 18). For four needles in the first set, D_1 was set to be a constant of 5 mm, while D_2 changed from 10 mm to 25 mm with an interval of 5 mm. For four needles in the second set, D_2 was set to be a constant of 25 mm, while D_1 changed from 5 mm to 20 mm with an interval of 5 mm. Due to the fact that a foil wore out quickly with the method presented in Section 3, a copper sheet was used instead to cut the slots, and the obtained slot width was 0.8 mm. The slot depth H was set to a constant of 0.75D. These two slot parameters actually also affect the frequency response of the needle and will be studied in the future. For each needle set, an additional needle was made as control (N5 and N10), which didn't have the two slots on the needle shaft. A summary of the needles in the two sets was shown in Tab. 2. Given that a needle can be approximated to be a homogeneous rod, the length of the needle L was determined using the following equation [15]:

$$L = \frac{c}{2f} \tag{1}$$

where c is the wave propagation speed of the material and defined as $c = \sqrt{E/\rho}$, and f is the target frequency of vibration (20 kHz in this case). In other words, L is the half wavelength of wave propagation in 304 stainless steel. With a Young's Module of 196 GPa and a density of 8000 kg/m^3, L was calculated as 123.7 mm.

Table 2. A summary of the needles in the experiment.

Set	Needle	D_1	D_2	Set	Needle	D_1	D_2
1	N1	5 mm	10 mm	2	N6	5 mm	25 mm
	N2		15 mm		N7	10 mm	
	N3		20 mm		N8	15 mm	
	N4		25 mm		N9	20 mm	
	N5		No slots		N10		No slots

To mitigate the effects of property variations of different porcine skin samples, each needle in a needle set was inserted into the same sample twice, once with vibration and once without. As a result, only 10 of the 12 holes were used for a skin sample. The average velocity of insertion was set to a constant of 1 mm/s for all the trials. Five trials were conducted for the vibration and the non-vibration condition of each needle respectively, and the force and position data were collected for each trial with a sampling rate of 1000 Hz. The averaged values of insertion force and depth were used in Section 5.

An example force-position plot is shown in Fig. 8, where three phases can be identified during the insertion process. In the first phase, the needle tip has not punctured the skin, and no cutting occurs. The force is mainly caused by the elastic deformation of the skin. In the second phase, the needle tip cuts and punctures and cuts through the skin. There is a significant drop in the force. The needle tip has exited the skin. The force is mainly caused by the friction between the needle shaft and the inner surface of puncture hole. Two parameters can be measured as the indicator of the performance of a needle. The first parameter is the puncture force, which is the peak value of insertion force before it suddenly drops. It is the maximum force the phantom endures before penetration begins. The second parameter is the puncture depth, which is defined as the insertion distance between 0.1N and the puncture force. It is related to the maximum deformation of the phantom during insertion. Both parameters are of great importance in evaluating the needle performance in practice, and keeping them low is usually preferred.

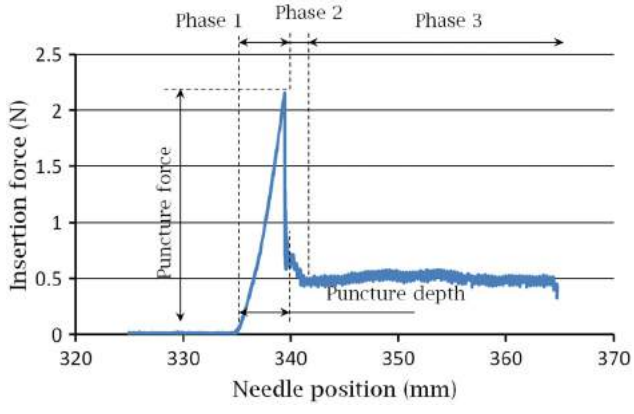

Figure 8. An example force-position plot in the skin phantom experiment.

4.3. Analytical modeling and vibration simulation

To determine the motion of the needle tip in air, a modal analysis study was conducted using the Simulation Add-in in SolidWorks (Concord, MA) software. The CAD

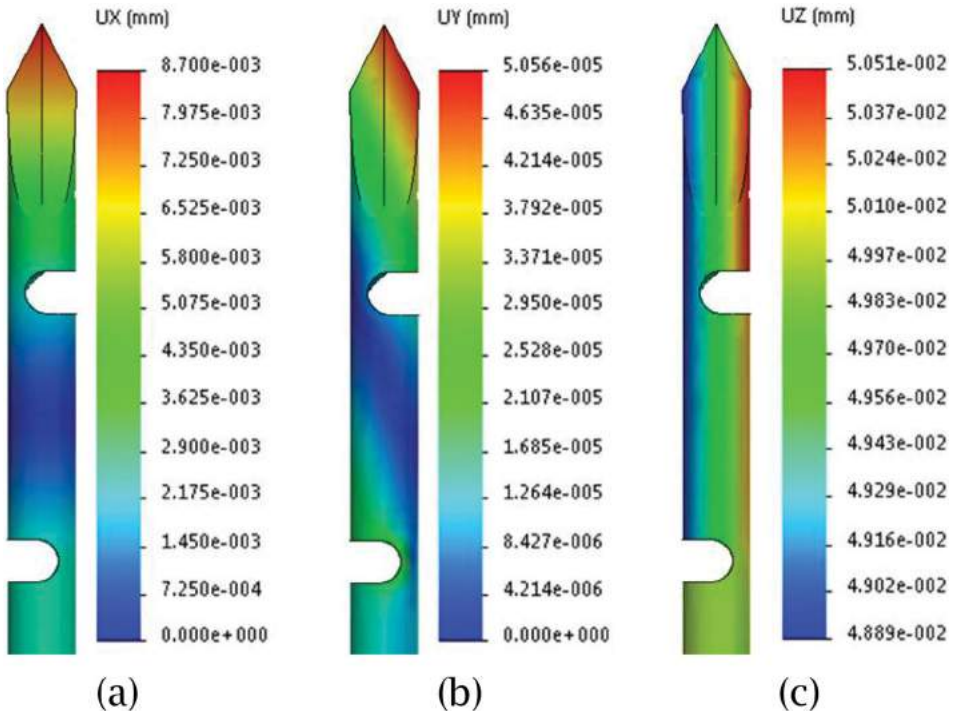

Figure 9. Mass normalized displacement of N1 in (a) X direction, (b) Y direction, and (c) Z direction.

models of the needle sets were built with the parameters shown in Tab. 2, and were meshed with a global size of 0.5 mm and a tolerance of 0.025 mm. Since the needle is in the free – free condition when attached to the end of the horn [24], no constraint was applied to the needle. An axial excitement with amplitude of 50 μm was applied at the bottom of the needle between the frequencies of 19 kHz and 21 kHz for harmonic analysis. As illustration, the deformation results of N1 as its displacements in the three directions at 20 kHz can be seen in Fig. 9(a-c). For all the needles in Tab. 2, the Z (axial) and X (transverse) direction displacement of the needle tip were recorded. The displacement in the Y direction was at the magnitude of 10^{-2}μm and thus not recorded.

5. Results and discussion

Fig. 10 shows the results of puncture force and depth for the first needle set under conditions with and without vibration. For each needle, the puncture forces and depths of the five trials were derived individually and averaged. For all the five needles, applying vibration resulted in the reduction in puncture force. N3 had the smallest values of puncture force for both conditions with and without vibration. The puncture depth also decreased, although it was not significant for N3. This is reasonable because the insertion force before puncture is caused by the elastic deformation of the testing medium. As the deformation increases, the insertion force also rises.

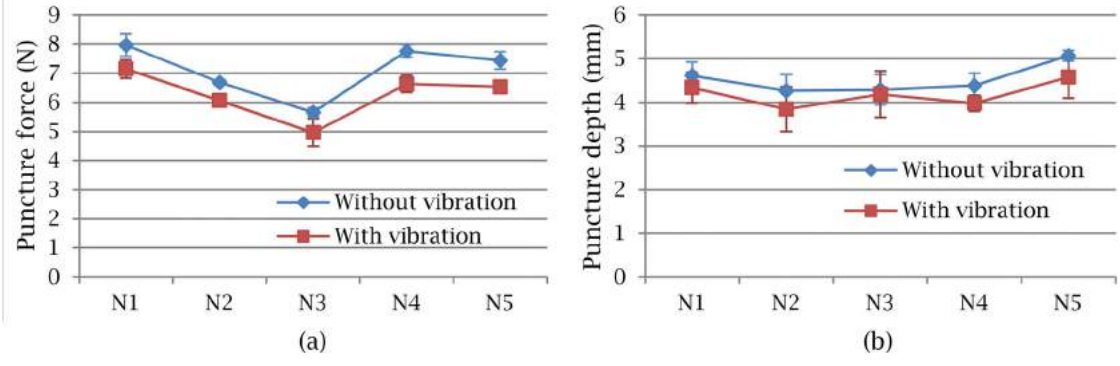

Figure 10. Experiment results for the first needle set: (a) puncture force and (b) puncture depth.

From Fig. 10, it can be noticed that when no vibration was applied, the puncture force and depth for the five needles were noticeably different from each other, while theoretically they should be the same or at least close to each other given the needles have identical φ and β. This may be due to the fact that the slots reduce the stiffness of the needle along the axial direction, so a greater displacement of the needle is needed to reach the required amount of force to puncture the porcine skin. Moreover, the front section of the needle is likely to bend slightly under force, so the tip is not interacting with the skin with its best perpendicular orientation. Another possibility is the minor geometry difference at the tips of the needles caused during fabrication. To better investigate the effects of D_1 and D_2 on needle performance, the relative decrease of puncture force was shown in Fig. 11. While N5 as control could reduce the puncture force by 12.2% after applying vibration, N1 to N4 can reduce by 10.3%, 11.5%, 12.3% and 14.5%, respectively. In other words, the proposed novel design of surgical needle can result in greater reduction in puncture force with proper selection of slot locations.

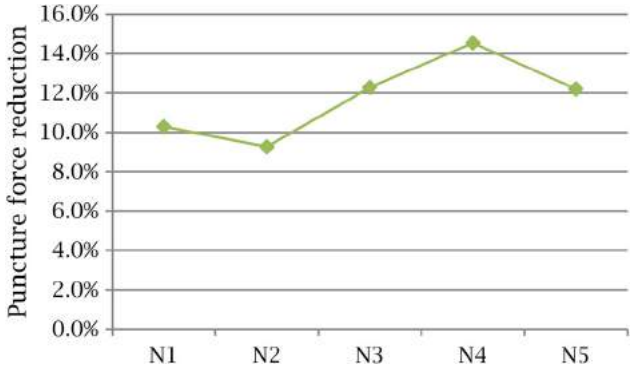

Figure 11. Relative reduction of puncture force for the first needle set.

Fig. 12 showed the mass normalized Z (axial) direction and X (transverse) direction displacement of the needle tip calculated in SolidWorks with excitement amplitude of 50 μm at 20 kHz for the first needle set. From N1 to N4, the Z displacement changed in the opposite trend to the X displacement. N2 had the largest X displacement and lowest Z displacement. N5 as control had virtually no X displacement, but a Z displacement at the magnitude of the excitement amplitude. For N1 to N4, the X displacement only changed between the range of 7.8 μm and 9.1 μm. From the design point of view, it indicated that for the given range changing D_2 alone had minor effects on transverse displacement. By comparing Fig. 12 and Fig. 11, it can be seen that for these four needles, a larger Z displacement resulted in greater reduction in puncture force, so the difference in the puncture force of this needle set seemed to be mainly determined by Z displacement. Although N5 had the largest Z displacement, its X displacement was almost zero. This should be the reason why it had a lower force reduction than N4.

Fig. 13 showed the results of puncture force and depth for the second needle set under conditions with and without vibration. Just like in the first set, applying vibration resulted in the reduction in both puncture force and depth, although the depth reduction for N8 was not significant. N8 had the smallest values of puncture force for both vibration conditions. The relative decrease of puncture force was shown in Fig. 14. While N10 as control could reduce the puncture force by 12.2% after applying vibration, N6 to N9 can reduce by 14.5%, 14.6%, 10.0% and 7.1%, respectively. For this needle set, the design of N6 and N7 can result in greater reduction in puncture force.

Fig. 15 showed the mass normalized Z and X direction displacement of the needle tip calculated in SolidWorks for the second needle set. Z displacement also went against the trend of X displacement. N8 had the

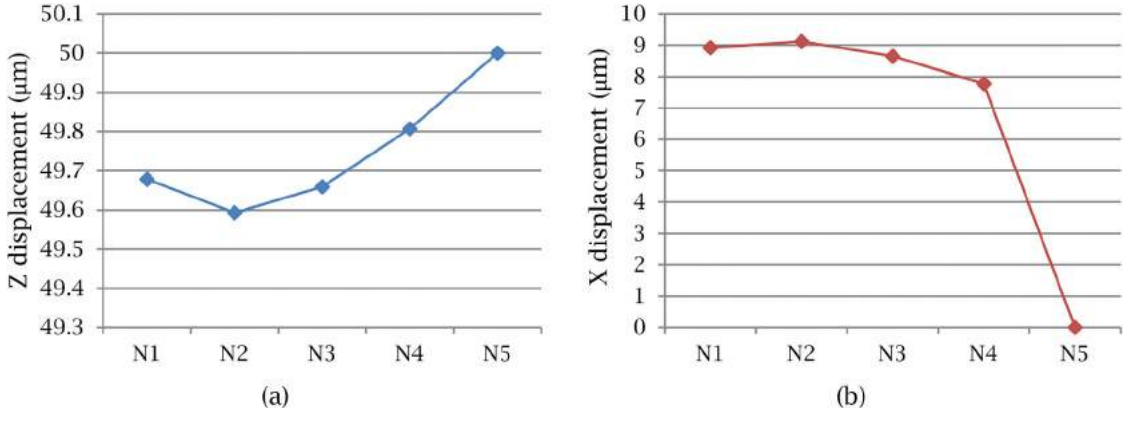

Figure 12. Mass normalized displacement of the first needle set in (a) Z direction and (b) X direction.

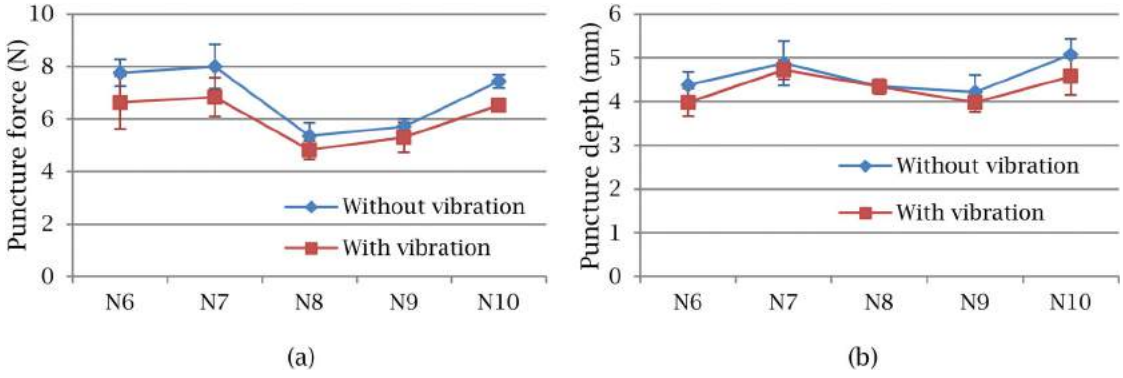

Figure 13. Experiment results for the second needle set: (a) puncture force and (b) puncture depth.

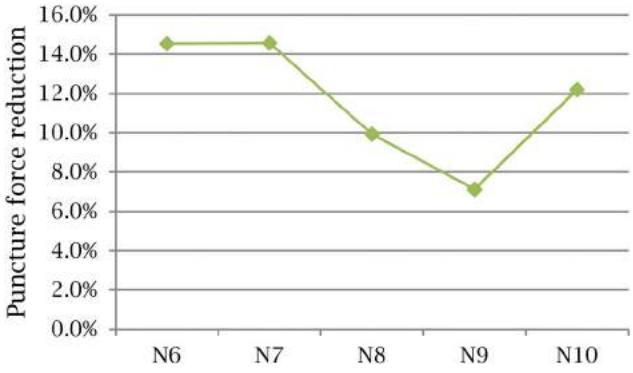

Figure 14. Relative reduction of puncture force for the second needle set.

largest X displacement and lowest Z displacement. N10 as control had a Z displacement at the magnitude of the excitement amplitude but virtually no X displacement. For N6 to N9, the X displacement changed between the range of 7.8 μm and 14.6 μm, which is greater than the range in the first needle set. From the design point of view, it indicated that for the given range changing D_1 had greater effects on transverse displacement than D_2. Since the X displacement changed more greatly, the puncture force didn't seem to be determined by Z displacement alone. The reduction of puncture force in Fig. 14 didn't show much similarity with Z displacement in Fig. 15(a) or X displacement in Fig. 15(b). However, if the X and Z displacement were combined like two perpendicular vectors as shown in Fig. 16, the new displacement matched the reduction of puncture force in Fig. 11. In other words, a larger combined amplitude of X and Z vibration would result in greater reduction of puncture force.

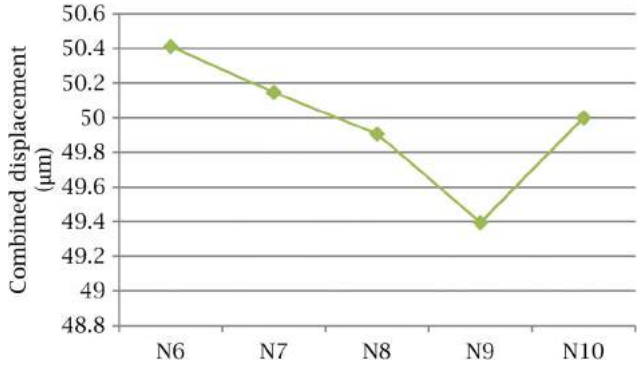

Figure 16. Combined displacement of Z and X direction for the second needle set.

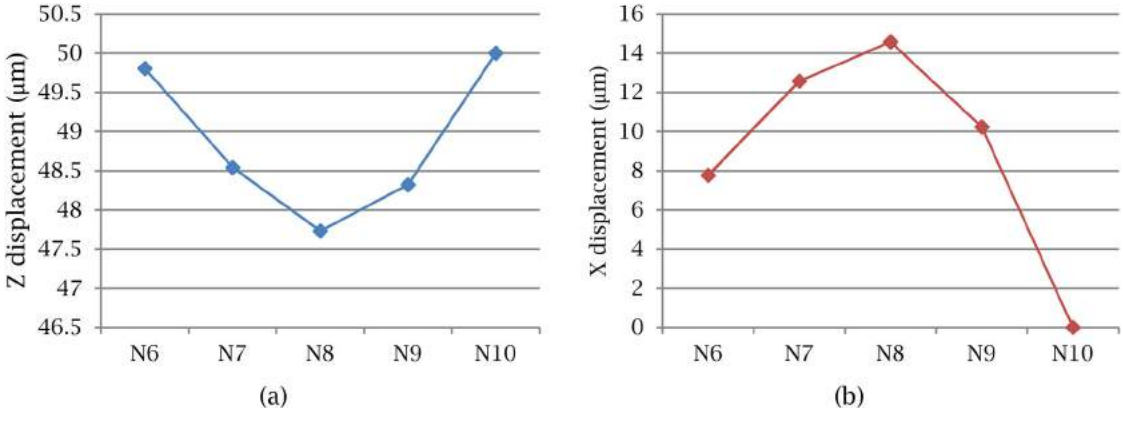

Figure 15. Mass normalized displacement of the second needle set in (a) Z direction and (b) X direction.

6. Conclusions and future work

This paper presents a novel design of solid surgical needle featured by its 4-bevel tip and shaft slots with the aim to further explore the potential of vibratory needle insertion for medical applications. The design philosophy was discussed, and the EDM processes for fabricating the needle were introduced. Prototypes of the needle design with different geometry parameters were fabricated and used for insertion into porcine skin with ultrasonic vibration. The results showed that the needle design could reduce the puncture force by 14.5% at maximum than the 12.2% of control. The reduction of puncture force was determined by the Z displacement and/or the combined X and Z displacement. From the design point of view, changing D_1 will be more effective in increasing transverse displacement than D_2 for the presented range.

Due to the factors such as uncontrollable needle fabrication repeatability and possible variations in porcine skin properties, the feasibility and effectiveness of the proposed compliant needle design was not yet well demonstrated. To better explore the potential of vibratory needle insertion and get more accurate results, the following improvements should be made in the future research. Duplicates of needles should be fabricated and used in experiments to minimize the influence of fabrication uncertainty. Materials with higher consistency should be used instead of porcine skin. The issues of stress and fatigue still remain to be studied. More needles with different geometry parameters (D_1, D_2 and H) will be tested.

Acknowledgement

This work was partially supported by the National Science Foundation (NSF) Grants (CMMI-1125872, CMMI-1404916 and CMMI-1547105) to North Carolina State University and the National Science Foundation (NSF) Grants (CMMI-1404916) to The Penn State University. Their support is greatly appreciated.

ORCID

Yi Cai http://orcid.org/0000-0002-7587-8956
Jason Moore http://orcid.org/0000-0002-8830-2833
Yuan-Shin Lee http://orcid.org/0000-0001-9892-5199

References

[1] Abolhassani, N.; Patel, R.; Moallem, M.: Needle insertion into soft tissue: A survey, Medical Engineering & Physics, 29(4), 2007, 413–431. http://dx.doi.org/10.1016/j.medengphy.2006.07.003

[2] Barnett, A. C.; Lee, Y.-S.; Moore, J. Z.: Fracture Mechanics Model of Needle Cutting Tissue, Journal of Manufacturing Science and Engineering, 138(1), 2015, 011005–011005. http://dx.doi.org/10.1115/1.4030374

[3] Barnett, A. C.; Wolkowicz, K.; Moore, J. Z.: Vibrating Needle Cutting Force, Proceedings of ASME 2014 International Manufacturing Science and Engineering Conference, Ann Arbor, Michigan, USA, 2014, V002T02A025-V002T02A025. http://dx.doi.org/10.1115/MSEC2014-4049

[4] Davis, S. P.; Landis, B. J.; Adams, Z. H.; Allen, M. G.; Prausnitz, M. R.: Insertion of microneedles into skin: measurement and prediction of insertion force and needle fracture force, Journal of biomechanics, 37(8), 2004, 1155–1163. http://dx.doi.org/10.1016/j.jbiomech.2003.12.010

[5] DiMaio, S. P.; Salcudean, S. E.: Needle insertion modeling and simulation, IEEE Transactions on Robotics and Automation, 19(5), 2003, 864–875. http://dx.doi.org/10.1109/TRA.2003.817044

[6] Egekvist, H.; Bjerring, P.; Arendt-Nielsen, L.: Pain and mechanical injury of human skin following needle insertions, European Journal of Pain, 3(1), 1999, 41–49. http://dx.doi.org/10.1016/S1090-3801(99)90187-8

[7] Heverly, M.; Dupont, P.; Triedman, J.: Trajectory Optimization for Dynamic Needle Insertion, IEEE International Conference on Robotics and Automation, 2005, 1646–651. http://dx.doi.org/10.1109/ROBOT.2005.1570349

[8] Huang, Y. C.; Tsai, M. C.; Lin, C. H.: A piezoelectric vibration-based syringe for reducing insertion force, IOP Conference Series: Materials Science and Engineering, 42(1), 2012, 012–020. http://dx.doi.org/10.1088/1757-899X/42/1/012020

[9] Khalaji, I.; Hadavand, M.; Asadian, A.; Patel, R. V.; Naish, M. D.: Analysis of needle-tissue friction during vibration-assisted needle insertion, Proceedings of IEEE/RSJ International Conference on Intelligent Robots and Systems (IROS), Tokyo, Japan, 2013, 4099–4104. http://dx.doi.org/10.1109/IROS.2013.6696943

[10] Kim, Y.-C.; Park, J.-H.; Prausnitz, M. R.: Microneedles for drug and vaccine delivery, Advanced drug delivery reviews, 64(14), 2012, 1547–1568. http://dx.doi.org/10.1016/j.addr.2012.04.005

[11] Kong, F.; Lee, Y.-S.: Analytical Modeling of Ultrasonic Vibration Assisted Drilling of Bones for Medical Surgical Applications, Proceedings of ASME 2015 International Manufacturing Science and Engineering Conference, Charlotte, North Carolina, USA, 2015, V002T03A008-V002T03A008. http://dx.doi.org/10.1115/MSEC2015-9488

[12] Liu, C.; Zhao, B.; Gao, G.; Zhang, X.: Study on ultrasonic vibration drilling of particulate reinforced aluminum matrix composites, Key Engineering Materials, 291, 2005, 447–452. http://dx.doi.org/10.4028/www.scientific.net/KEM.291-292.447

[13] Mahvash, M.; Dupont, P. E.: Fast needle insertion to minimize tissue deformation and damage, Proceeding of IEEE International Conference on Robotics and Automation, Kobe, Japan, 2009, 3097–3102. http://dx.doi.org/10.1109/robot.2009.5152617

[14] Maurin, B.; Barbe, L.; Bayle, B.; Zanne, P.; Gangloff, J.; De Mathelin, M.; Gangi, A.; Soler, L.; Forgione A.,: In vivo study of forces during needle insertions, Proceedings of the medical robotics, navigation and visualisation scientific workshop, 2004, 1–8. http://dx.doi.org/10.1142/9789812702678_0056

[15] Meirovitch, L., Analytical methods in vibration. The Mcmillan Company, New York, NY, 1967.
[16] Moore, J. Z.; Malukhin, K.; Shih, A. J.; Ehmann, K. F.: Hollow needle tissue insertion force model, CIRP Annals - Manufacturing Technology, 60(1), 2011, 157–160. http://dx.doi.org/10.1016/j.cirp.2011.03.101
[17] Moore, J. Z.; McLaughlin, P. W.; Shih, A. J.: Novel needle cutting edge geometry for end-cut biopsy, Medical Physics, 39(1), 2012, 99–108. http://dx.doi.org/10.1118/1.3665253
[18] Moore, J. Z.; Zhang, Q.; McGill, C. S.; Zheng, H.; McLaughlin, P. W.; Shih, A. J.: Modeling of the Plane Needle Cutting Edge Rake and Inclination Angles for Biopsy, Journal of Manufacturing Science and Engineering, 132(5), 2010, 051005–051005. http://dx.doi.org/10.1115/1.4002190
[19] O'Leary, M. D.; Simone, C.; Washio, T.; Yoshinaka, K.; Okamura, A. M.: Robotic needle insertion: effects of friction and needle geometry, Proceedings of IEEE International Conference on Robotics and Automation, Taipei, Taiwan, 2003, 1774–1780. http://dx.doi.org/10.1109/ROBOT.2003.1241851
[20] Okamura, A. M.; Simone, C.; O'Leary, M. D.: Force modeling for needle insertion into soft tissue, IEEE Transactions on Biomedical Engineering, 51(10), 2004, 1707–1716. http://dx.doi.org/10.1109/TBME.2004.831542
[21] Podder, T.; Clark, D.; Sherman, J.; Fuller, D.; Messing, E.; Rubens, D.; Strang, J.; Zhang, Y.; O'Dell, W.; Ng, W.: Effects of tip geometry of surgical needles: an assessment of force and deflection, Proceedings of International Federation of Medical and Biological Engineering, 2005, 1727–1983. http://odell.radonc.med.ufl.edu/papers/EMBS05_Podder_needleForces.pdf
[22] Podder, T.; Sherman, J.; Fuller, D.; Messing, E.; Rubens, D.; Strang, J.; Brasacchio, R.; Yu, Y.: In-vivo measurement of surgical needle intervention parameters: a pilot study, Proceedings of 28th Annual International Conference of the IEEE Engineering in Medicine and Biology Society, New York City, New York, USA, 2006, 3652–3655. http://dx.doi.org/10.1109/IEMBS.2006.259917
[23] Pujana, J.; Rivero, A.; Celaya, A.; de Lacalle, L. L.: Analysis of ultrasonic-assisted drilling of Ti6Al4 V, International Journal of Machine Tools and Manufacture, 49(6), 2009, 500–508. http://dx.doi.org/10.1016/j.ijmachtools.2008.12.014
[24] Seah, K.; Wong, Y.; Lee, L.: Design of tool holders for ultrasonic machining using FEM, Journal of Materials Processing Technology, 37(1), 1993, 801–816. http://dx.doi.org/10.1016/0924-0136(93)90138-V
[25] Takeyama, H.; Kato, S.: Burrless drilling by means of ultrasonic vibration, CIRP Annals-Manufacturing Technology, 40(1), 1991, 83–86. http://dx.doi.org/10.1016/S0007-8506(07)61939-8
[26] Wang, Y.; Chen, R. K.; Tai, B. L.; McLaughlin, P. W.; Shih, A. J.: Optimal needle design for minimal insertion force and bevel length, Medical Engineering & Physics, 36(9), 2014, 1093–1100. http://dx.doi.org/10.1016/j.medengphy.2014.05.013
[27] Webster, R. J.; Kim, J. S.; Cowan, N. J.; Chirikjian, G. S.; Okamura, A. M.: Nonholonomic modeling of needle steering, The International Journal of Robotics Research, 25(5-6), 2006, 509–525. http://dx.doi.org/10.1177/0278364906065388
[28] Yang, M.; Zahn, J. D.: Microneedle insertion force reduction using vibratory actuation, Biomedical microdevices, 6(3), 2004, 177–182. http://dx.doi.org/10.1023/B:BMMD.0000042046.07678.2e